VIP Solar Cells

DOI: 10.1002/anie.200904492

Optical Fiber/Nanowire Hybrid Structures for Efficient Three-Dimensional Dye-Sensitized Solar Cells**

*Benjamin Weintraub, Yaguang Wei, and Zhong Lin Wang**

Renewable and green energy are the technological drivers of the future economy. Solar cells (SCs) are one of the most important sustainable energy technologies that have the potential to meet the world's energy demands.[1] Among the various approaches to SCs,[2–11] the performance of dye-sensitized solar cells (DSSCs) is largely influenced by the surface area of adsorbed light-harvesting molecules. Traditional DSSCs utilize a nanoparticle film for enhancing the SC conversion efficiency.[12,13] Photons absorbed by the dye monolayer create excitons that are rapidly split at the surface of the nanoparticles. After splitting, electrons are injected into the nanoparticles and holes move towards the opposite electrode by means of a redox species in an electrolyte. The surface area of the nanoparticle film and the effectiveness of charge collection by the electrodes determine the photovoltaic efficiency of the cell. The latter property has been improved by using aligned ZnO nanowire (NW) arrays, which provide direct electrical pathways for rapid collection of carriers generated throughout the device, and a full-sun efficiency of 1.5% has been demonstrated.[14] However, the design is still based on a two-dimensional (2D) planar substrate, which has a relatively low surface area that limits the dye loading capacity and restricts mobility and adaptability for remote operation. Moreover, the increasing surface area is limited by the requirement that the electron transport distance d remains significantly smaller than the electron diffusion length L_n in order to minimize recombination of electrons with holes or other species. For wire-based SCs, in which light is illuminated perpendicular to the wire,[15,16] the shadow effect from the entangled wire shaped electrode may limit the enhancement in power efficiency.

We report herein an innovative hybrid structure that integrates optical fibers and nanowire (NW) arrays as three-dimensional (3D) dye-sensitized solar cells (DSSCs) that have a significantly enhanced energy conversion efficiency. The ZnO NWs grow normal to the optical fiber surface and enhance the surface area for the interaction of light with dye molecules. The light illuminates the fiber from one end along the axial direction, and its internal reflection within the fiber creates multiple opportunities for energy conversion at the interfaces. In comparison to the case of light illumination normal to the fiber axis from outside the device (2D case), the internal axial illumination enhances the energy conversion efficiency of a rectangular fiber-based hybrid structure by a factor of up to six for the same device. Furthermore, the absolute full-sun efficiency (AM 1.5 illumination, 100 mW cm^{-2}) is increased to 3.3%, which is 120% higher than the highest value reported for ZnO NWs grown on a flat substrate surface and 47% higher than that of ZnO NWs coated with a TiO_2 film. This research demonstrates a new approach from 2D to 3D solar cells with advantages of high efficiency, expanded mobility, surface adaptability, and concealed/remote operation capability.

The DSSC hybrid structure is an integrates optical fibers and ZnO NWs grown by a chemical approach on the fiber surfaces. The design principle is shown in Figure 1. The main structure consists of a bundle of quartz fibers arranged such

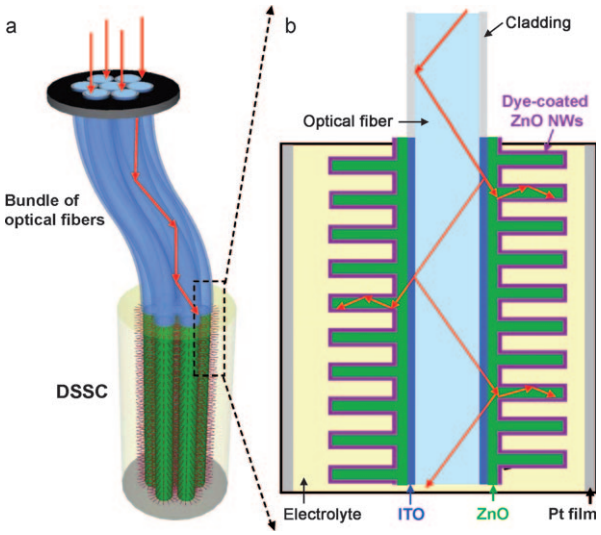

Figure 1. Design and principle of a three-dimensional DSSC. The cross-section of the fiber can be cylindrical or rectangular. a) The 3D DSSC is composed of optical fibers and ZnO NWs are grown vertically on the fiber surface. The top segment of the bundled optical fibers utilizes conventional optical fibers and allows for remote transmission of light. The bottom segment consists of the 3D DSSC for solar power generation at a remote/concealed location. b) Detailed structure of the 3D DSSC.

[*] B. Weintraub,[+] Dr. Y. Wei,[+] Prof. Z. L. Wang
School of Materials Science and Engineering
Georgia Institute of Technology
771 Ferst Drive, Atlanta, GA 30332(USA)
Fax: (+1) 404-894-9140
E-mail: zlwang@gatech.edu

[+] These authors contributed equally to this work.

[**] Research supported by DARPA (Army/AMCOM/REDSTONE AR, W31P4Q-08-1-0009), BES DOE (DE-FG02-07ER46394), Air Force Office (FA9550-08-1-0446), DARPA/ARO W911NF-08-1-0249, KAUST Global Research Partnership, NSF (DMS0706436, CMMI 0403671). B.W. thanks IPST at Georgia Tech for fellowship support. The authors thank Prof. Yulin Deng, Chen Xu, Zhou Li, and Dr. Rusen Yang for discussions and technical assistance.

Supporting information for this article is available on the WWW under http://dx.doi.org/10.1002/anie.200904492.

© 2009 Wiley-VCH Verlag GmbH & Co. KGaA, Weinheim

that the incident sunlight can enter the fibers from one end (Figure 1a). The upper region of the fibers functions to effectively guide light for concealed and adaptable applications. The fiber surface is coated with a low-refractive-index cladding layer for minimizing light loss. The DSSC is fabricated on the lower region of the fiber surface, which can be situated remotely from the top surface where incoming light enters the fiber. This segment of the fiber, which lacks a cladding layer, is first coated with an indium tin oxide (ITO) layer that simultaneously acts as a conductive electrode and a high-refractive-index material that allows light to escape the fiber and enter the DSSC (Figure 1b). A thin layer of ZnO deposited on the ITO layer serves as a seed layer for growth of aligned ZnO NWs by a chemical approach (Figures S1 and S2 in the Supporting Information).[17] The key principle is that the light entering from the axial direction inside the fiber experiences multiple internal reflections along the fiber. At each internal reflection at the fiber/ITO/ZnO NW interfaces, light will cross the interface to reach the dye molecules through the NWs. The effective propagation distance of light along the fiber covered with NWs is a few centimeters (Figures S3 and S4 in the Supporting Information). Therefore, the light interaction surface area is increased not only because of the NWs,[18] but also because of the multiple reflections along the fiber. This effect does not increase the path length that electrons must travel to reach the electrode, and is the core principle behind the 3D DSSC.

The 3D DSSC was fabricated as follows. Firstly, ZnO NW arrays were synthesized by a wet-chemical method on seeded, ITO layer-coated optical fibers. Next, the arrays were sensitized in a 0.5 mM N719 dye solution[19] in dry ethanol for one hour. The fiber was then cleaved using an optical fiber cleaver to achieve smooth surfaces and ensure efficient light coupling into the fiber. A Pt layer evaporated on a precleaned glass substrate served as the counterelectrode. The working electrode fiber coated with sensitized ZnO NWs was placed in parallel with the Pt film counterelectrode. The internal space of the device was filled with a liquid electrolyte (0.5 M LiI, 50 mM I_2, 0.5 M 4-tertbutylpyridine in 3-methoxypropionitrile) by the capillary effect. The entire cell was fully packaged and covered to prevent light leakage.

To first demonstrate the 3D DSSC concept, a cell was fabricated on a cylindrical optical fiber. ZnO NWs with lengths of approximately 15 μm were synthesized on a quartz fiber with a diameter of 0.2 mm (Figure 2a,b). The DSSC was investigated by using a single fiber placed in parallel with a flat Pt counterelectrode. Two typical configurations were considered: light illumination normal to the fiber axis (NA) and parallel to the fiber axis (PA), as shown in Figure 2c (insets). For the PA case, careful measurements were taken in order to eliminate light leakage at the fiber entrance (see Figure 1a) and accurately calculate the illumination cross-sectional area. The plot of current density against voltage (J–V curve) shows the open circuit voltage V_{OC}, short-circuit current density J_{SC}, fill factor FF, and energy conversion efficiency $\eta = FF \times V_{OC} \times J_{SC}/P_{in}$, where P_{in} is the incident light power density. It is apparent that the axial illumination configuration yields an enhanced efficiency. To properly characterize the enhancement in energy conversion efficiency, the efficiency enhancement factor EEF is defined as the ratio of power efficiencies for the PA and NA cases, that is, $EEF = \eta_{PA}/\eta_{NA}$. For a total of five DSSCs, the EEF ranges from 4 to 18 (Figure 2d). The large value is partially due to the hybrid structure and partially to the geometrical configuration of the Pt film electrode.[20] Most importantly, this result provides proof of the design concept presented in Figure 1 for a 3D DSSC. The short-circuit current density J_{SC} for the PA case is much higher than that for the NA case, while the open-circuit voltage V_{OC} for the PA case is significantly lower than that for the NA case. This difference occurs as the lower local incident light intensity at the ZnO–dye interface is lower in the PA case than in the NA case because of multiple internal reflections in the fiber (see Figure 4a).

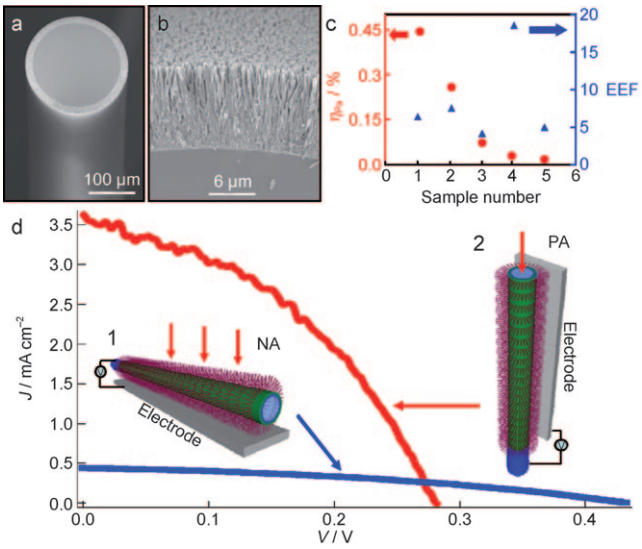

Figure 2. Cylindrical optical-fiber-based 3D DSSC and its performance. a) Low-magnification SEM image of a quartz fiber with uniformly grown ZnO NWs on its surface. b) High-magnification SEM image showing the densely packed ZnO NWs on the fiber surface. c) Plot of EEF and the corresponding energy conversion efficiencies for five 3D DSSCs. The data variation is mainly attributed to fluctuations in SC packaging. d) J–V curves of the DSSC under one full-sun illumination (AM 1.5 illumination, 100 mW cm^{-2}). The illumination is 1) normal to the fiber axis (NA; 2D case) and 2) parallel to the fiber axis (PA; 3D case). For the NA case, $J_{sc} = 0.44$ mA cm^{-2}, $V_{oc} = 0.433$ V, FF = 0.375, $\eta_{NA} = 0.071$ %. For the PA case, $J_{sc} = 3.73$ mA cm^{-2}, $V_{oc} = 0.283$ V, FF = 0.414, $\eta_{PA} = 0.44$ %. A corresponding efficiency enhancement factor of EEF = 6.1 has been achieved by converting the 2D DSSC to 3D DSSC.

However, the absolute efficiency of the cylindrical fiber in the PA case is still limited (Figure 2d), mainly by the curved geometry of the fiber and the short mean free path of the generated charges (case 2 in Figure 2d). The highest efficiency we have achieved with this configuration is 0.45 %. The flat Pt film electrode can effectively collect the photon-induced holes created at the side surface of the fiber adjacent to the electrode, but the holes generated at the opposite surface may not reach the electrode before recombining with electrons or other species.[13] An ideal solution to capture all of the holes is to use a cylindrical, tube-shaped electrode to

 © 2009 Wiley-VCH Verlag GmbH & Co. KGaA, Weinheim

enclose the fiber, but this design is difficult to achieve in practice with DSSCs. An improved design takes advantage of the rectangular optical fiber geometry.

The motivation for using a rectangular fiber is the gain in effective contact area between the fiber and the flat Pt electrode for efficient collection of photon-induced holes in the electrolyte. ZnO NWs can be grown uniformly on all four sides of a fiber (see Figure S5 in the Supporting Information), but accurate comparison of the performance of the NA and PA cases shows that long NWs of lengths around 25 μm[21] and diameter 200 nm were grown on only three sides of the fiber (Figure 3a,b). In the NA illumination case (case 1 in Figure 3d), which was designed to be similar to a 2D DSSC arrangement, the uncovered top surface of the fiber allows light to effectively penetrate into the fiber and reach the bottom surface, where NWs meet the Pt electrode, thus resulting in a typical energy conversion efficiency. If the top surface of the fiber had been covered by NWs, the incident light would have been significantly attenuated once it reached the bottom surface, thus resulting in a reduction in energy conversion efficiency and thus an erroneous representation of a 2D DSSC. The PA measurement was conducted using the same hybrid-structured fiber, except that the light was introduced from the end (case 2 in Figure 3d). The *J*–*V* curve shows a substantial difference between the two cases; most notably, the PA case has a significantly enhanced current density. For a total of eight devices, the efficiency of the 3D design for the PA case is enhanced by a factor of up to six (Figure 4d). The absolute energy conversion efficiency

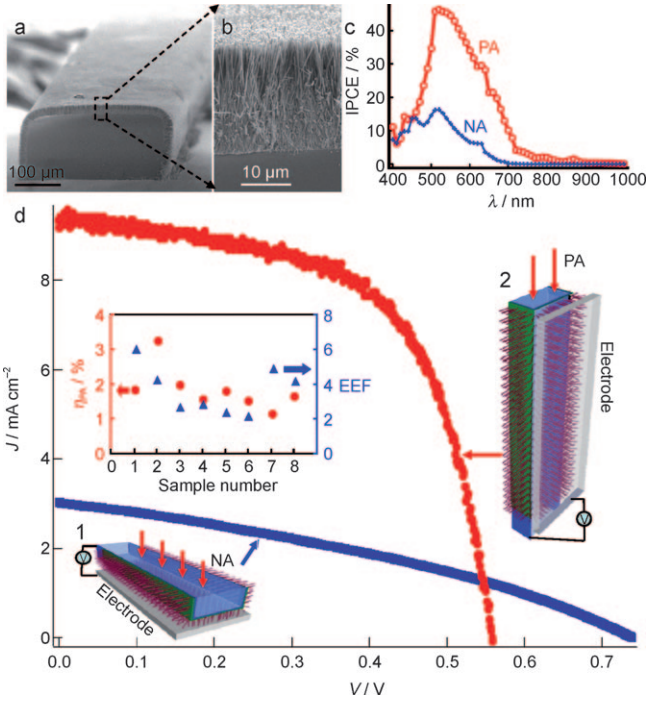

Figure 3. Rectangular optical-fiber-based 3D DSSC and its performance. a) Low-magnification SEM image of a quartz fiber with uniformly grown ZnO NWs on three sides. b) High-magnification SEM image showing the densely packed ZnO NWs on the fiber surface. c) Typical incident photon to electron conversion efficiency (IPCE) measured for the PA and NA cases from a DSSC. d) Current density *J* and voltage *V* curves of a DSSC under one full-sun illumination oriented 1) normal to the fiber axis (NA; 2D case) and 2) parallel to the fiber axis (PA; 3D case). For the NA case, $J_{sc}=3.02$ mA cm^{-2}, $V_{oc}=0.739$ V, $FF=0.342$, $\eta_{NA}=0.76\%$. For the PA case, $J_{sc}=9.5$ mA cm^{-2}, $V_{oc}=0.559$ V, FF = 0.623, $\eta_{PA}=3.3\%$. A corresponding efficiency enhancement factor of EEF = 4.34 has been achieved by converting the 2D DSSC to the 3D DSSC. The inset shows a plot of EEF and the corresponding energy conversion efficiencies for eight 3D DSSCs. The data variation is mainly attributed to fluctuations in SC packaging (see Table S1 in the Supporting Information).

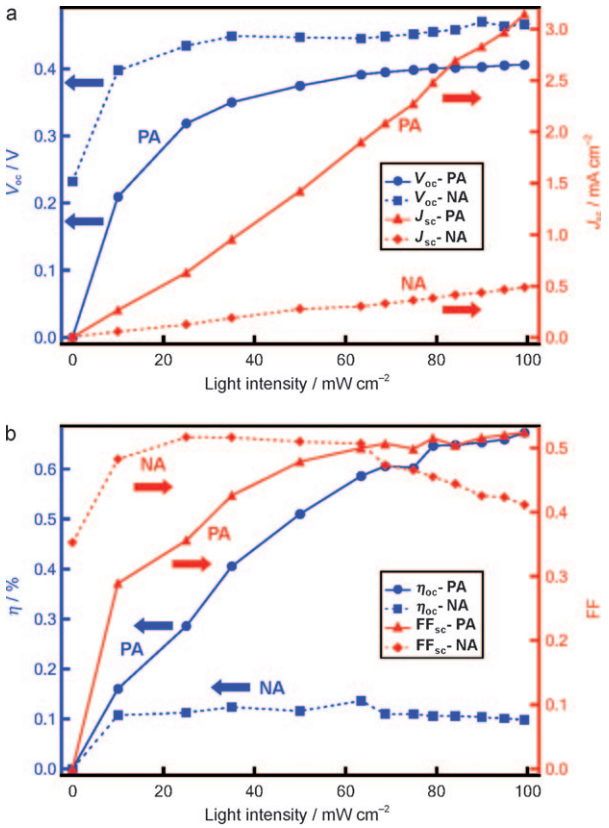

Figure 4. Characterization of a rectangular fiber-based 2D and 3D DSSC as a function of incident light intensity, showing the superior performance of the 3D DSSC. a) Dependence of the open-circuit voltage V_{oc} and short-circuit current density J_{sc} on incident light intensity for the NA and PA cases. b) Dependence of energy conversion efficiency and fill factor on incident light intensity for the NA and PA cases, demonstrating the largely enhanced performance of the 3D DSSC under weak light intensity to high light intensity (see Figure S6 in the Supporting Information).

reached as high as 3.3%, which is 120% higher than the reported value for ZnO NW DSSCs.[14] The one side of the fiber without NWs may contribute to the power conversion by serving as a mirror that reflects the light back towards the DSSC side. A drastic increase in energy conversion efficiency is therefore demonstrated when changing from the 2D illumination (NA case) to the 3D illumination (PA case).

The incident photon to electron conversion efficiencies (IPCE) or external quantum efficiency (EQE) for the PA and NA illumination cases were measured (Figure 3d, inset). Although the PA and NA orientations both exhibit maxima at 520 nm that correspond to the absorption maximum of the

 © 2009 Wiley-VCH Verlag GmbH & Co. KGaA, Weinheim

N719 dye, the PA orientation has a substantially larger absolute peak maximum compared to that of the NA curve (47% and 17%, respectively), thus further supporting the efficiency enhancement generated from the PA orientation. In addition, a broader photoaction in the red region is seen in the PA orientation, thus suggesting that longer-wavelength photons can be more efficiently converted to electrons farther down the optical fiber where the overall light intensity is diminished.

The superior performance of the PA configuration over the NA configuration can be investigated by examining the output characteristics of the DSSC as a function of incident light intensity. The open-cell voltage is significantly higher for the NA case than for the PA case (Figure 4a) because the local light intensity at the ZnO–dye interface is lower in the PA case than in NA case. Also, the current density in the PA case is a lot larger than that in the NA case and increases linearly with light intensity. This result indicates that the multiple light reflections within the fiber play a role in enhancing the current output. It is noted that the efficiency of the NA case is rather flat, which is consistent with the result in reference [14], but the efficiency of the PA case increases linearly (Figure 4b), possibly because of the multiple reflections of the stronger light with an intensity above the threshold for receiving detectable solar power generation in the fiber. The energy conversion efficiency at one full sun for the PA case is much larger than that for the NA case. In addition, the fill factor of the NA case decreases with light intensity, while that of the PA case maintains a steadily increasing trend. These data show that the performance of the DSSC in the PA configuration outperforms that of the NA case from intensities of one full sun and below. The short-circuit current density in the PA case increases linearly and does not reach a saturation maximum until an incident light intensity of over 10 full suns (Figure S6 in the Supporting Information), thus showing the potential of our system for applications under intensively focused sun light.

The use of fiber-based media for fabricating SCs is a natural choice. A fiber-shaped organic photovoltaic cell has been demonstrated by utilizing concentric thin films of small molecular organic compounds.[22] The cell is illuminated at normal incidence to the fiber axis through a thin metal electrode, and exhibits a power conversion efficiency of 0.5%. Organic photovoltaic devices have been fabricated on multimode optical fibers by constructing concentric thin films.[23] An energy conversion efficiency of 0.6% has been measured under parallel-to-axial illumination. Our approach is based on a hybrid structure that integrates an optical fiber and aligned ZnO NW arrays, which increases the light-absorbing surface area because of multiple reflections and the presence of the nanostructure. The efficiency of the 3D DSSC is enhanced by up to a factor of six compared to the 2D DSSC. The 3D DSSC, which is based on pure ZnO NWs, yields a full-sun energy conversion efficiency of up to 3.3%, which is 120% higher than the efficiency received using ZnO NWs on a flat substrate surface (for a review see reference [24]), 47% higher than that produced using ZnO NWs coated with TiO_2,[25] 15 times higher than that of the hybrid polymer/ZnO NW photovoltaic devices ($\eta = 0.2\%$),[26] and even higher than that of the SCs made using TiO_2 nanotube arrays ($\eta = 2.9\%$)[27] and SCs based on CdSe quantum wires/dots ($\eta = 2.9\%$).[6,7] The performance strongly suggests that the paradigm shift from 2D to 3D DSSCs offers a general approach for the development of high-efficiency SCs.

The 3D DSSC has the several outstanding features. From a physical perspective, the 2D DSSC based on NWs has a low surface area, which limits dye loading. Attempts at increasing the surface area by maximizing NW length are restricted to NW dimensions much smaller than the electron diffusion length ($d \ll L_n$). The 3D DSSC is advantageous because this configuration allows light to have multiple interactions with the dye molecules without increasing the electron transport distance d. The 3D design has the following key merits for applications. Firstly, the use of fibers allows the DSSC to function remotely with high mobility. The SC unit can be concealed and located where the sunlight is available away from the surface, thus making unique designs and surface-confined applications possible. Secondly, the design concept transforms the traditional SC from action at the light illuminated side surface (e.g., 2D or projection area) to action inside the volume (e.g., 3D) of the unit, therefore allowing applications at remote locations such as underground and in deep water, in which light arrives at an exterior surface but the SC is concealed elsewhere. To produce the same amount of electricity, the 3D DSSC could have a smaller size, greater mobility, more robust design, flexible shape, and potentially lower production cost. Thirdly, the 3D DSSC has a high saturation limit and large dynamic range so that it works effectively from low light intensities below 1 sun (Figure 4) to very high light intensities (>10 suns; Figure S6 in the Supporting Information). Furthermore, the 3D DSSC processing utilizes chemical synthesis at low temperatures with environmentally friendly and biologically safe materials,[28] with a great potential for scale-up. Finally, since ZnO NWs can be grown on substrates of any material or shape at temperatures below 100 °C,[29] it is possible to replace the quartz optical fibers with highly transparent polymer fibers. By combining the hybrid structure presented here with new dyes and surface coating materials, it is possible to significantly improve the efficiency of DSSCs in general. Our method provides a new and general approach for designing high-performance SC using organic and inorganic materials.

Experimental Section

Fiber preparation: Circular fibers were provided by OFS Optics (HCS 200). To expose the 200 μm pure silica core, the ETFE (ethylene tetrafluoroethylene) jacket was mechanically stripped and the polymer cladding (HCS) was removed with acetone. Rectangular fibers were home-made by grinding circular quartz rods into a rectangular geometry with a 2:1 aspect ratio. The rods were drawn into fiber strands under an oxygen-enriched flame. All fibers were ultrasonically cleaned in acetone, water, and ethanol. Thin films of 300 nm ITO and 50 nm ZnO were deposited by radio frequency (RF) magnetron sputtering at room temperature. For circular fibers, the samples were oriented parallel to the sputtering target on a rotating sample stage for uniform coverage of all surfaces. For three-side-coated rectangular fibers, samples were oriented normal to the sputter target to result in thin films on only three sides. NWs were

 © 2009 Wiley-VCH Verlag GmbH & Co. KGaA, Weinheim

synthesized by a wet-chemical method in a Pyrex glass bottle containing 20 mM zinc chloride (Aldrich) and 20 mM hexamine (Fluka) at 95 °C for 16 h in a Yamato convection box oven. Aspect ratios were controlled by adding (0–5 mL in 100 mL solutions) 28 % ammonium hydroxide (Aldrich). All chemicals were reagent grade. Samples were rinsed with water and ethanol and air-dried at 95 °C for 12 h. Fiber tips were cleaved with a Corning diamond fiber cleaver (the manufacturer guarantees fiber end-faces that average less than 0.7° from the perpendicular), which ensured efficient light coupling into the fiber. The fibers were characterized on a LEO 1550 field-emission gun SEM.

3D DSSC fabrication: The NW arrays were sensitized in a 0.5 mM N719 dye solution in dry ethanol for 1 h.[30] A Pt layer was evaporated on a precleaned glass substrate with a Ti adhesion layer that served as the counterelectrode. The working electrode fiber coated with sensitized ZnO NWs was placed in parallel with the Pt film counterelectrode. The internal space of the device was filled with a liquid electrolyte (0.5 M LiI, 50 mM I_2, 0.5 M 4-tertbutylpyridine in 3-methoxypropionitrile (Fluka)) by the capillary effect. The entire cell was fully packaged and shielded to prevent light leakage.

3D DSSC output measurements: The solar cell was irradiated using a solar simulator (300 W Model 91160, Newport) with an AM 1.5 spectrum distribution calibrated against a NREL reference cell to accurately simulate a full-sun intensity (100 mW cm^{-2}). The *J*–*V* curve was measured under two configurations: light illumination normal to the fiber axis (NA) and parallel to the fiber axis (PA; Figure 2d and Figure 3d). For the PA case, the optical fiber was completely shielded by black scotch tape except for the tip, where light could couple with the fiber. IPCE measurements were carried out using a 300 W Xe lamp light source coupled to a monochromator (Oriel). A reference Si photodiode calibrated for spectral response was used for the monochromatic power-density calibration. Intensity-dependent measurements below 1.4 full-sun intensity were carried out with a set of neutral density filters and by adjusting the input power of the solar simulator. To increase the light intensity up to 14 suns for high intensity solar measurements, two converging lenses were placed in between the light source and the DSSC. The light attenuation along the fiber was measured using the solar simulator as the source in conjunction with color filters of wavelength 400 nm, 500 nm, 550 nm, 700 nm, and 880 nm, respectively and a thermopile as the photodetector. The same fiber was tested at different lengths.

Received: August 12, 2009
Published online: October 22, 2009

Keywords: dyes/pigments · energy conversion · nanostructures · optical fibers · solar cells

[1] M. S. Dresselhaus, I. L. Thomas, *Nature* **2001**, *414*, 332.
[2] B. Z. Tian, X. L. Zheng, T. J. Kempa, Y. Fang, N. F. Yu, G. H. Yu, J. L. Huang, C. M. Lieber, *Nature* **2007**, *449*, 885.
[3] G. Yu, J. Gao, J. C. Hummelen, F. Wudl, A. J. Heeger, *Science* **1995**, *270*, 1789.
[4] J. J. M. Halls, C. A. Walsh, N. C. Greenham, E. A. Marseglia, R. H. Friend, S. C. Moratti, A. B. Holmes, *Nature* **1995**, *376*, 498.
[5] B. O'Regan, M. Grätzel, *Nature* **1991**, *353*, 737.
[6] W. U. Huynh, J. J. Dittmer, A. P. Alivisatos, *Science* **2002**, *295*, 2425.
[7] I. Gur, N. A. Fromer, M. L. Geier, A. P. Alivisatos, *Science* **2005**, *310*, 462.
[8] P. Peumans, S. Uchida, S. R. Forrest, *Nature* **2003**, *425*, 158.
[9] J. Y. Kim, *K.* Lee, N. E. Coates, D. Moses, T. Q. Nguyen, M. Dante, A. J. Heeger, *Science* **2007**, 317, 222.
[10] A. Goetzberger, C. Hebling, H. W. Schock, *Mater. Sci. Eng. R* **2003**, *40*, 1.
[11] C. J. Brabec, N. S. Sariciftci, J. C. Hummelen, *Adv. Mater.* **2001**, *11*, 15.
[12] M. Grätzel, *Nature* **2001**, *414*, 338.
[13] J. Bisquert, D. Cahen, G. Hodes, S. Ruhle, A. Zaban, *J. Phys. Chem. B* **2004**, *108*, 8106.
[14] M. Law, L. E. Greene, J. C. Johnson, R. Saykally, P. D. Yang, *Nat. Mater.* **2005**, *4*, 455.
[15] M. R. Lee, R. D. Eckert, K. Forberich, G. Dennler, C. J. Brabec, R. A. Gaudiana, *Science* **2009**, *324*, 232.
[16] X. Fan, Z. Chu, F. Wang, C. Zhang, L. Chen, Y. Tang, D. Zou, *Adv. Mater.* **2008**, *20*, 592.
[17] Y. Qin, X. D. Wang, Z. L. Wang, *Nature* **2008**, *451*, 809.
[18] The effective surface area or roughness factor (RF) is defined as the total film area per unit substrate. The measured RF is 267 for the three-sided rectangular fiber and 196 for the circular fiber. RF was measured by UV/Vis spectroscopy by desorbing the dye in an alkaline aqueous solution. The calculation of the roughness factor for the NA case is straightforward because the incident light intensity is fairly uniform across the illumination area. For the PA case, the intensity of the incident light decays as the light travels along the axis. The calculated roughness factor may not truly affect the roughness factor.
[19] X. Kakiuchi, E. Hosono, S. Fujihara, *J. Photochem. Photobiol. A* **2006**, *179*, 81.
[20] The electrode was fabricated by depositing a thin film of Pt on a glass substrate. The configuration of the Pt counterelectrode is important for deciding the collection efficiency of the holes. The flat Pt electrode can effectively collect the holes generated at the bottom surface of the fiber adjacent to the electrode, but the holes generated at the upper surface may not reach the electrode before recombining with electrons and/or other species in electrolyte. Moreover, in such a design configuration, the most effective power generation portion is the upper part of the fiber that directly faces the sunlight, while the sunlight is largely attenuated once it penetrates through the ZnO NWs, ITO layer, and fiber to reach the bottom surface of the fiber. This attenuation is part of the reason that the EEF is high but the absolute energy conversion efficiency is low for this configuration.
[21] We found experimentally that the longer NWs resulted in higher efficiencies. NW arrays around 25 μm in length were the longest we grew by using a chemical approach. However, superlong NWs usually form a dense film adjacent to the fiber because of the lateral growth of the NWs.
[22] B. O'Connor, K. P. Pipe, M. Shtein, *Appl. Phys. Lett.* **2008**, *92*, 193306.
[23] J. W. Liu, M. A. G. Namboothiry, D. L. Carroll, *Appl. Phys. Lett.* **2007**, *90*, 063501.
[24] I. Gonzalez-Valls, M. Lira-Cantu, *Energy Environ. Sci.* **2009**, *2*, 19.
[25] M. Law, L. E. Greene, A. Radenovic, T. Kuykendall, J. Liphardt, P. D. Yang, *J. Phys. Chem. B* **2006**, *110*, 22652.
[26] P. Ravirajan, A. M. Peiro, M. K. Nazeeruddin, M. Graetzel, D. C. C. Bradley, J. R. Durrant, J. Nelson, *J. Phys. Chem. B* **2006**, *110*, 7635.
[27] G. K. Mor, K. Shankar, M. Paulose, O. K. Varghese, C. A. Grimes, *Nano Lett.* **2006**, *6*, 215.
[28] Z. Li, R. Yang, M. Yu, F. Bai, C. Li, Z. L. Wang, *J. Phys. Chem. C* **2009**, *112*, 20114.
[29] Z. L. Wang, *Mater. Sci. Eng. R* **2009**, *64*, 33.
[30] K. Kakiuchi, E. Hosono, S. Fujihara, *J. Photochem. Photobiol. A* **2006**, *179*, 81.

 © 2009 Wiley-VCH Verlag GmbH & Co. KGaA, Weinheim